Biomedical Optics EXPRESS

Nanoparticle-free tissue-mimicking phantoms with intrinsic scattering

Maciej S. Wróbel,[1] Alexey P. Popov,[2] Alexander V. Bykov,[2] Valery V. Tuchin,[2,3,4,5] and Małgorzata Jędrzejewska-Szczerska[1,*]

[1]*Gdańsk University of Technology, Faculty of Electronics, Telecommunications and Informatics, Department of Metrology and Optoelectronics, Gabriela Narutowicza Str. 11/12, 80-233 Gdańsk, Poland*
[2]*University of Oulu, Faculty of Information Technology and Electrical Engineering, Optoelectronics and Measurement Techniques Laboratory, P.O. Box 4500, FI-90014 Oulu, Finland*
[3]*Saratov National Research State University, Research-Education Institute of Optics and Biophotonics, 410012 Saratov, Russia*
[4]*Institute of Precision Mechanics and Control of Russian Academy of Sciences, 410028 Saratov, Russia*
[5]*National Research Tomsk State University, Laboratory of Biophotonics, 634050 Tomsk, Russia*
[*]*mjedrzej@eti.pg.gda.pl*

Abstract: We present an alternative to the conventional approach, phantoms without scattering nanoparticles, where scattering is achieved by the material itself: spherical cavities trapped in a silicone matrix. We describe the properties and fabrication of novel optical phantoms based on a silicone elastomer polydimethylsiloxane (PDMS) and glycerol mixture. Optical properties (absorption coefficient μ_a, reduced scattering coefficient μ_s', and anisotropy factor g) of the fabricated phantoms were retrieved from spectrophotometric measurements (in the 400–1100 nm wavelength range) using the inverse adding-doubling method. The internal structure of the phantoms was studied under a scanning electron microscope, and the chemical composition was assessed by Raman spectroscopy. Composition of the phantom material is reported along with the full characterization of the produced phantoms and ways to control their parameters.

OCIS codes: (170.7050) Turbid media; (160.4760) Optical properties; (160.4670) Optical materials; (170.3660) Light propagation in tissues; (160.0160) Materials; (170.0170) Medical optics and biotechnology.

References and links

1. V. O. Korhonen, T. S. Myllyla, M. Y. Kirillin, A. P. Popov, A. V. Bykov, A. V. Gorshkov, E. A. Sergeeva, M. Kinnunen, and V. Kiviniemi, "Light propagation in NIR spectroscopy of the human brain," IEEE J. Sel. Top. Quantum Electron. **20**(2), 289 (2014).
2. N. C. Dingari, I. Barman, G. P. Singh, J. W. Kang, R. R. Dasari, and M. S. Feld, "Investigation of the specificity of Raman spectroscopy in non-invasive blood glucose measurements," Anal. Bioanal. Chem. **400**(9), 2871–2880 (2011).
3. V. V. Tuchin, A. N. Bashkatov, E. A. Genina, V. I. Kochubey, V. V. Lychagov, S. A. Portnov, N. A. Trunina, D. R. Miller, S. Cho, H. Oh, B. Shim, M. Kim, J. Oh, H. Eum, Y. Ku, D. Kim, and Y. Yang, "Finger tissue model and blood perfused skin tissue phantom," Proc. SPIE **7898**, 78980Z (2011).
4. M. Nemati, G. B. Loozen, N. van der Wekken, G. van de Belt, H. P. Urbach, N. Bhattacharya, and S. Kenjeres, "Application of full field optical studies for pulsatile flow in a carotid artery phantom," Biomed. Opt. Express **6**(10), 4037–4050 (2015).
5. N. Spegazzini, I. Barman, N. C. Dingari, R. Pandey, J. S. Soares, Y. Ozaki, and R. R. Dasari, "Spectroscopic approach for dynamic bioanalyte tracking with minimal concentration information," Sci. Rep. **4**, 7013 (2014).
6. J. Chaiken, J. Goodisman, B. Deng, R. J. Bussjager, and G. Shaheen, "Simultaneous, noninvasive observation of elastic scattering, fluorescence and inelastic scattering as a monitor of blood flow and hematocrit in human fingertip capillary beds," J. Biomed. Opt. **14**(5), 050505 (2009).
7. K. Karpienko, M. Gnyba, D. Milewska, M. S. Wróbel, and M. Jędrzejewska-Szczerska, "Blood equivalent phantom vs whole human blood, a comparative study," J. Innov. Opt. Health Sci. **9**(5), 1650012 (2015).
8. I. Feder, H. Duadi, and D. Fixler, "Experimental system for measuring the full scattering profile of circular phantoms," Biomed. Opt. Express **6**(8), 2877–2886 (2015).
9. I. Barman, N. C. Dingari, N. Rajaram, J. W. Tunnell, R. R. Dasari, and M. S. Feld, "Rapid and accurate determination of tissue optical properties using least-squares support vector machines," Biomed. Opt. Express **2**(3), 592–599 (2011).

#260393 Received 2 Mar 2016; revised 16 Apr 2016; accepted 28 Apr 2016; published 4 May 2016

10. A. V. Bykov, A. P. Popov, A. V. Priezzhev, and R. Myllylä, "Multilayer tissue phantoms with embedded capillary system for OCT and DOCT imaging," Proc. SPIE **8091**, 80911R (2011).
11. A. V. Bykov, A. P. Popov, M. Kinnunen, T. Prykäri, A. V. Priezzhev, and R. Myllylä, "Skin phantoms with realistic vessel structure for OCT measurements," Proc. SPIE **7376**, 73760F (2010).
12. D. Fixler and R. Ankri, "Subcutaneous gold nanorods [corrected] detection with diffusion reflection measurement," J. Biomed. Opt. **18**(6), 061226 (2013).
13. M. S. Wróbel, M. Jedrzejewska-Szczerska, S. Galla, L. Piechowski, M. Sawczak, A. P. Popov, A. V. Bykov, V. V. Tuchin, and A. Cenian, "Use of optical skin phantoms for preclinical evaluation of laser efficiency for skin lesion therapy," J. Biomed. Opt. **20**(8), 085003 (2015).
14. E. A. Barnoy, D. Fixler, R. Popovtzer, T. Nayhoz, and K. Ray, "An ultra-sensitive dual-mode imaging system using metal-enhanced fluorescence in solid phantoms," Nano Res. **8**(12), 3912–3921 (2015).
15. I. Barman, G. P. Singh, R. R. Dasari, and M. S. Feld, "Turbidity-corrected Raman spectroscopy for blood analyte detection," Anal. Chem. **81**(11), 4233–4240 (2009).
16. G. Lamouche, B. F. Kennedy, K. M. Kennedy, C.-E. Bisaillon, A. Curatolo, G. Campbell, V. Pazos, and D. D. Sampson, "Review of tissue simulating phantoms with controllable optical, mechanical and structural properties for use in optical coherence tomography," Biomed. Opt. Express **3**(6), 1381–1398 (2012).
17. B. W. Pogue and M. S. Patterson, "Review of tissue simulating phantoms for optical spectroscopy, imaging and dosimetry," J. Biomed. Opt. **11**(4), 041102 (2006).
18. M. S. Wróbel, A. P. Popov, A. V. Bykov, M. Kinnunen, M. Jędrzejewska-Szczerska, and V. V. Tuchin, "Multi-layered tissue head phantoms for noninvasive optical diagnostics," J. Innov. Opt. Health Sci. **8**(03), 1541005 (2015).
19. R. C. Chang, P. Johnson, C. M. Stafford, and J. Hwang, "Fabrication and characterization of a multilayered optical tissue model with embedded scattering microspheres in polymeric materials," Biomed. Opt. Express **3**(6), 1326–1339 (2012).
20. S. E. Bohndiek, S. Bodapati, D. Van De Sompel, S.-R. Kothapalli, and S. S. Gambhir, "Development and Application of Stable Phantoms for the Evaluation of Photoacoustic Imaging Instruments," PLoS One **8**(9), e75533 (2013).
21. T. Moffitt, Y.-C. Chen, and S. A. Prahl, "Preparation and characterization of polyurethane optical phantoms," J. Biomed. Opt. **11**(4), 041103 (2006).
22. B. F. Kennedy, S. Loitsch, R. A. McLaughlin, L. Scolaro, P. Rigby, and D. D. Sampson, "Fibrin phantom for use in optical coherence tomography," J. Biomed. Opt. **15**(3), 030507 (2010).
23. D. Fixler, T. Nayhoz, and K. Ray, "Diffusion reflection and fluorescence lifetime imaging microscopy study of fluorophore-conjugated gold nanoparticles or nanorods in solid phantoms," ACS Photonics **1**(9), 900–905 (2014).
24. R. Ankri, H. Taitelbaum, and D. Fixler, "Reflected light intensity profile of two-layer tissues: phantom experiments," J. Biomed. Opt. **16**(8), 085001 (2011).
25. C. Iliescu, H. Taylor, M. Avram, J. Miao, and S. Franssila, "A practical guide for the fabrication of microfluidic devices using glass and silicon," Biomicrofluidics **6**(1), 016505 (2012).
26. D. M. de Bruin, R. H. Bremmer, V. M. Kodach, R. de Kinkelder, J. van Marle, T. G. van Leeuwen, and D. J. Faber, "Optical phantoms of varying geometry based on thin building blocks with controlled optical properties," J. Biomed. Opt. **15**(2), 025001 (2010).
27. X. Wen, Z. Mao, Z. Han, V. V. Tuchin, and D. Zhu, "In vivo skin optical clearing by glycerol solutions: mechanism," J. Biophotonics **3**(1-2), 44–52 (2010).
28. A. Ron, N. Racheli, I. Breskin, and R. Shechter, "A tissue mimicking phantom model for applications combining light and ultrasound," Proc. SPIE **8583**, 858307 (2013).
29. M. S. Wróbel, A. P. Popov, A. V. Bykov, M. Kinnunen, M. Jędrzejewska-Szczerska, and V. V. Tuchin, "Measurements of fundamental properties of homogeneous tissue phantoms," J. Biomed. Opt. **20**(4), 045004 (2015).
30. E. Mendelovici, R. L. Frost, and T. Kloprogge, "Cryogenic Raman spectroscopy of glycerol," J. Raman Spectrosc. **31**(12), 1121–1126 (2000).
31. D. Cai, A. Neyer, R. Kuckuk, and H. M. Heise, "Raman, mid-infrared, near-infrared and ultraviolet–visible spectroscopy of PDMS silicone rubber for characterization of polymer optical waveguide materials," J. Mol. Struct. **976**(1-3), 274–281 (2010).
32. A. N. Bashkatov, E. A. Genina, and V. V. Tuchin, "Optical properties of skin, subcutaneous, and muscle tissues: a review," J. Innov. Opt. Health Sci. **04**(01), 9–38 (2011).
33. E. A. Genina, A. N. Bashkatov, and V. V. Tuchin, "Optical clearing of cranial bone," Adv. Opt. Technol. **2008**, e267867 (2008).
34. B. C. Quirk, R. A. McLaughlin, A. M. Pagnozzi, B. F. Kennedy, P. B. Noble, and D. D. Sampson, "Optofluidic needle probe integrating targeted delivery of fluid with optical coherence tomography imaging," Opt. Lett. **39**(10), 2888–2891 (2014).

1. Introduction

Rapid growth in the field of optical measurement techniques for medical imaging, diagnosis and therapeutics requires the use of tissue-mimicking objects. Such objects called optical phantoms are fabricated to reduce usage of real biological tissues and resemble them by their optical properties. Nowadays, optical techniques are receiving rising interest as non-invasive

#260393 Received 2 Mar 2016; revised 16 Apr 2016; accepted 28 Apr 2016; published 4 May 2016

tools for medical diagnostics. Detecting clinical-level changes in the parameters of bodily fluids, such as intracranial cerebrospinal fluid pressure [1], blood glucose levels [2,3], microvasculature blood flow rates [4] as well as the parameters of the blood itself [5–7] are of great importance and are extensively studied. Optical phantoms are used mainly for calibration and development of these optical measurement and imaging systems [8,9]. They serve as reference standards for comparison of devices and techniques as well as for studying light transport in complex, often multi-layered tissues or organs with internal vasculature [10,11]. Also phantom studies of nanoparticles for skin cancer diagnosis and laser therapy has been reported [12,13]. A multitude of different types of phantoms have been invented to suit the needs of specific research methods, such as fluorescence [14] or Raman [15] imaging. While the scattering and absorption properties are the primary parameters of every phantom, their other properties define their usefulness in specific applications. Properties such as their lifetime stability, flexibility, low cost, short manufacture times, homogeneity, ease of production and possibility to create complex systems with internal inhomogeneities, such as capillaries or microchannels are greatly sought after.

Phantoms are composed of matrix material, scattering constituent, and absorbing constituent. This allows for independent and rigorous control of absorption and scattering. There are two main groups of phantoms depending on the means to achieve their light scattering properties: nano- or microparticle-induced scattering, and intrinsic scattering of the used materials. Achieving desired scattering coefficient in nano- or microparticle-based phantoms is controlled through the nanoparticle type, size, shape, and concentration. Particles such as titanium dioxide [16], aluminum oxide [17], zinc oxide [18] or polymer microspheres [19] have been used. The most common matrix materials in which the particles are suspended are: polyvinylchloride-plastisol [20], polyurethane and polyester resin [21], silicone and other materials [17]. This is a widely accepted and the most common approach. However, in many cases, the sedimentation or clustering of nanoparticles causes uncontrolled inhomogeneity of phantom properties due to uneven distribution of scattering centers. Methods which solve these problems require additional equipment, increase the time, cost, and difficulty of phantom fabrication. The particle-free phantoms, with intrinsic scattering, are perfectly homogeneous and usually easier to produce. Some phantoms fabricated this way used collagen, agarose, or even fibrin matrix [22] to encapsulate scattering Intralipid solution. However, a drawback of such phantoms with intrinsic scattering lies in their short lifetime and reduced possibilities for introducing structures and creating multiple layers [23,24].

We present a new design for fabrication of particle-free optical phantoms with intrinsic scattering arising from the matrix material itself. This phantom has homogeneous optical properties, long lifetime of months, is stable at room temperature, flexible, inexpensive, easy to produce and to control scattering properties during manufacturing process. The phantom comprises a silicone elastomer polydimethylsiloxane (PDMS) mixed with glycerol. Both composing materials are transparent in the VIS-NIR wavelength range. This mixture creates an emulsion which is stable after curing. We have retrieved the absorption coefficient μ_a, reduced scattering coefficient μ_s' and anisotropy factor g of the produced phantoms. Altering the optical properties of phantoms was achieved during the manufacture procedure by changing the content of glycerol in the mixture. The phantoms are designed as stable, flexible phantoms with the possible introduction of structural inhomogeneities. This composition of materials is reported for the first time to the best of the author's knowledge, along with full characterization of the produced phantoms and ways to control their parameters.

2. Materials and methods

We describe the procedure for the phantom fabrication, as well as describe the materials that make up the phantom. We later describe the methods used for characterization of the phantom internal structure, as well as its chemical composition, and the resulting optical properties.

#260393 Received 2 Mar 2016; revised 16 Apr 2016; accepted 28 Apr 2016; published 4 May 2016

2.1 Materials and phantom fabrication process

The bulk of the phantom comprises two materials, first of which is a silicone elastomer polydimethylsiloxane (PDMS). The PDMS (Sylgard® 184, Dow Corning, USA) is a two-component organic silicone which cures at room temperature over 48 hours. Heating effectively reduces curing time to minutes. This allows for creation of complex, multilayer systems with internal structures. PDMS has been widely used as a material for fabrication of microfluidics devices [25] due to its hydrophobicity after curing, which permits creation of microchannels. PDMS is transparent in the VIS-NIR, non-toxic, and non-flammable. Although PDMS was previously used for phantom fabrication it was always used as a matrix material forming PDMS-particulate mixture [26], never as a particle-free scattering phantoms. The other material used in the mixture is glycerol (1,2,3-propanetriol). Glycerol (≥ 99.5% Sigma-Aldrich) is a viscous, transparent liquid. It is used in the field of biophotonics primarily as an optical clearing agent [27] in various optical techniques, but it was also used as a matrix material for liquid, particle-based phantoms [28].

The phantom fabrication procedure is as follows: first, the two components of PDMS were mixed together according to the manufacturers' proposed quantities of 10:1 parts by volume, a ratio of the base PDMS material to the curing agent volumes. Then, required amount of glycerol was applied and carefully, thoroughly mixed, not to introduce excessive amounts of air. Air was evacuated from the mixture in a vacuum chamber. The mixture was poured into rectangular aluminum molds with controlled thickness. The standard process of the phantom fabrication requires no heating, as mixture is left at room temperature to solidify in less than 24 hours. Phantoms fabricated this way were primarily used to study their internal structure and measure their optical properties. Later we introduced changes in the procedure to control the optical properties of phantoms by varying the amount of glycerol in the mixture.

2.2 Methods for characterization of materials

The characterization of the phantom morphology and chemical structure was conducted by scanning electron microscopy and Raman spectroscopy.

A scanning electron microscope (SEM) (JCM-5000, JEOL, Japan) was used to image the internal structure of the phantoms. This gave us the opportunity to identify the origin of the intrinsic scattering. Introduced changes in the internal composition dependent on the amount of glycerol were observed under SEM. Phantoms were cut into pieces and placed in the chamber to observe their inner structure.

To identify chemical substances by their fingerprint Raman spectrum, which is unique for each substance, we used a Raman system (Nomadic, BaySpec) with three different excitation wavelengths: 532 nm, 785 nm and 1064 nm, of which 785 nm was the most useful. Raman spectra were smoothed for clarity and baseline-corrected. We studied a sample of glycerol, a transparent phantom (solidified PDMS) and a scattering PDMS-glycerol mixture phantom. Comparison of the recorded spectra enabled identification of the chemical composition of the cavities.

2.3 Measurements of optical properties

For retrieval of the optical properties of the phantoms we have followed a previously described procedure [18,29], which utilized the inverse adding-doubling (IAD) calculations based on spectrophotometric measurements. For this, we used the OL-750 spectrophotometer system with integrating spheres (Optronic Laboratories, USA) to measure total transmittance T, diffuse reflectance R, and collimated transmittance CT of the phantoms in the wavelength range of 400-1100 nm. Measurements over 2 weeks proved stability of their parameters.

We have used the spectral-domain optical coherence tomograph OCT Hyperion (Thorlabs, USA) for measuring the phantoms geometrical thickness. The phantoms were cut in half and placed on a glass slide. We calculated their thickness by the division of the optical to the geometrical thickness of the phantom.

#260393 Received 2 Mar 2016; revised 16 Apr 2016; accepted 28 Apr 2016; published 4 May 2016

The refractive index (RI) of the phantoms was measured at 450 nm, 589 nm, 680 nm, 800 nm, 930 nm and 1100 nm using an Abbe refractometer (DR-M2 1550, Atago, Japan). These values were used to retrieve the optical properties of phantoms in the IAD method.

3. Results and discussion

The study of the phantom internal structure and chemistry proved to establish the origin of the internal scattering of the fabricated phantoms as arising from the refractive index mismatch between the matrix medium PDMS and the cavities partially filled by glycerol. SEM images of phantoms (Fig. 1) illustrate their internal structure. The cavity size histograms (Fig. 2(a)-2(e)) show that increasing concentration of glycerol causes their size distribution to shift towards larger sizes, and an increase of the total area A_c occupied by the cavities (Fig. 2(f)).

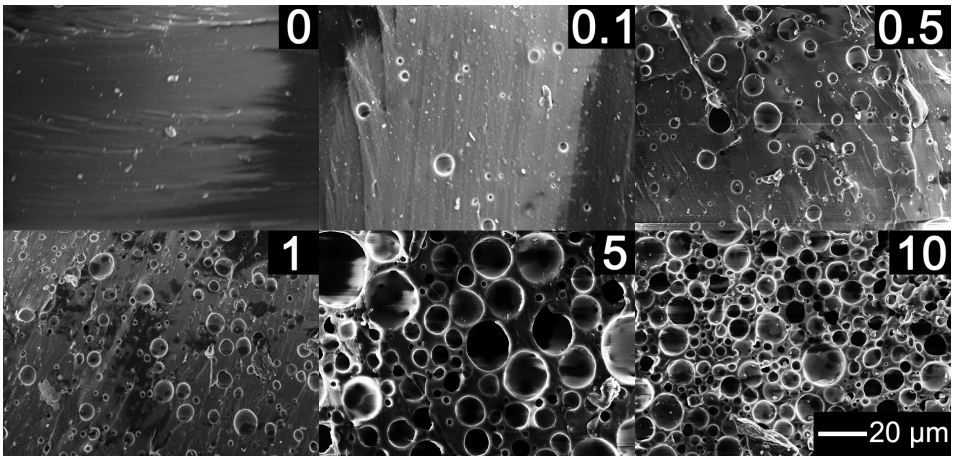

Fig. 1. SEM images of the internal structure of phantoms with different glycerol concentrations from 0 to 10 parts per volume, mixed with 10:1 parts per volume of PDMS to the curing agent.

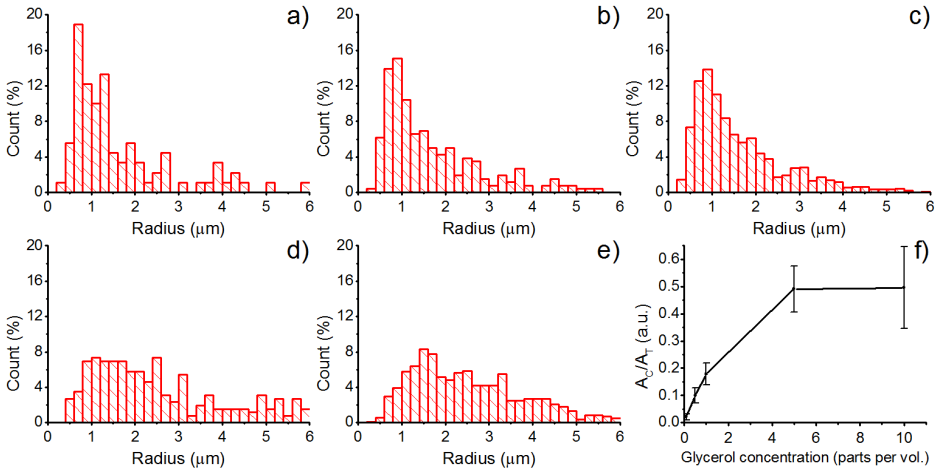

Fig. 2. Size distribution histograms for each glycerol concentration from 0.1 to 10 parts per volume (a)-(e); Ratio of the area occupied by cavities A_c to the total area A_T vs. glycerol concentration (f). Each experimental point in (f) corresponds to histograms from (a) to (e), respectively.

The study of chemical composition of the phantom was carried out to obtain information about the content of the cavities. The presence of spectral lines only from both glycerol [30] and PDMS [31] in the phantom spectrum proves that PDMS polymerization was unaffected by the addition of glycerol and that no chemical reaction occurred between the PDMS and

#260393 Received 2 Mar 2016; revised 16 Apr 2016; accepted 28 Apr 2016; published 4 May 2016

glycerol (Fig. 3). Therefore the resulting phantom is an emulsion formed of glycerol-filled micron-sized cavities suspended in the PDMS matrix.

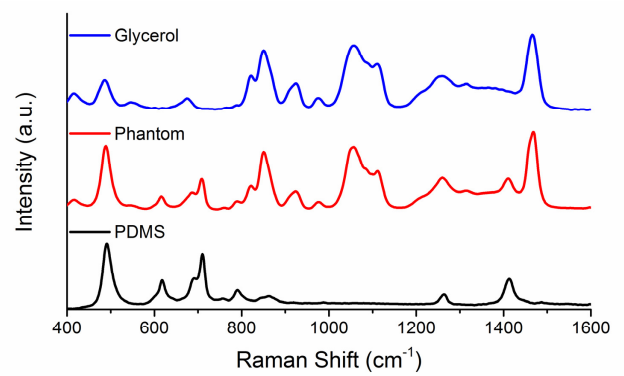

Fig. 3. Raman spectra of glycerol (top), phantom (middle) and PDMS (bottom).

Retrieved optical properties of the phantoms are presented in Fig. 4. The reduced scattering coefficient decreases with the wavelength. The introduction of higher concentrations of glycerol results in formation of more cavities and of larger diameters which increases the μ_s' of the phantoms (see Fig. 4(c)). However, when the glycerol constitutes over 25% of the total phantom volume (see Fig. 1, glycerol concentration from 5 to 10 parts), the cavities occupy more and more space with creation of new cavities with a broader size distribution (see Fig. 2 from (d) to (e)) resulting in scattering dependence saturation at high glycerol concentrations. This practically limits the possible μ_s' which can be achieved at values of about 3.5 mm^{-1} at 500 nm and 2.5 mm^{-1} at 1100 nm. Results are reproducible, yet some batch-to-batch variation is present during the production of the phantoms which is illustrated by the error bars in Fig. 4(c).

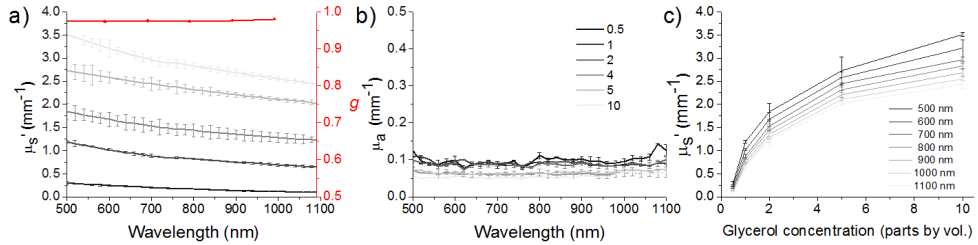

Fig. 4. Dependence of μ_s', g, (a) and μ_a (b) on the wavelength and the glycerol content (shown in the legend) in the produced phantoms; Measured μ_s' at different wavelengths and glycerol concentrations in the produced phantoms (c).

Comparison of the cavity-occupied area A_c to the total area A_T ratio (Fig. 2(f)) and μ_s' (Fig. 4(c)) dependent on the glycerol concentration shows a matching trend, which proves the origin of the intrinsic scattering. Our further study of optical clearing on these phantoms proves that cavities are filled up by air-glycerol mixture, with glycerol having refractive index (for λ = 589 nm) of 1.473 ± 0.001, thus the effective RI of the cavities is lower than 1.411 ± 0.001 of surrounding PDMS. Additionally, the absorption coefficient is smaller than 0.090 mm^{-1} ± 0.025 for all phantoms and remains constant in the whole wavelength range. Introduction of glycerol does not introduce any additional absorption. We have also measured the *g*-factor of these phantoms (Fig. 4(a)) which equals 0.975 ± 0.01 on average over the whole studied wavelength range.

The retrieved optical properties corresponding to many biological tissues [32]. Therefore, we suggest the possible application of our phantoms as primarily bone [33] and lung tissue [34], due to similar porosity of their morphology. Additionally we perceive them to be used as

#260393 Received 2 Mar 2016; revised 16 Apr 2016; accepted 28 Apr 2016; published 4 May 2016

an intermediate or connective medium between layers, or as a specific material for internal structures or inclusions. Capillaries are also a possible addition which allows for more complex, accurate and versatile tissue-mimicking possibilities e.g. in blood flow studies. The capabilities of optical phantoms to mimic specific tissues arise due to the ability to rigorously and independently control their scattering and absorption properties. They are usually fabricated with the use of particles suspended in a matrix material. Optical properties of particles, their size distribution and concentration define the scattering properties of phantoms. This approach has been widely used, however it has several disadvantages, such as particle sedimentation, clustering, and errors during the procedure cause inhomogeneities affecting phantom optical properties. Our presented phantoms with intrinsic scattering cause no such problems and offer several advantages: they are homogeneous, with controllable parameters, can be easily shaped and are elastic. This makes the PDMS-glycerol phantoms a viable new approach for creating optical tissue-mimicking phantoms, and testing optical clearing agents.

Acknowledgments

This study was partially supported by the Polish National Science Center under the grant 2011/03/D/ST7/03540, DS funds of the Faculty of Electronics, Telecommunications and Informatics, Gdańsk University of Technology; FiDiPro project 40111/11, TEKES, as well as COST Action BM1205. AB and AP acknowledge support provided by the Academy of Finland (290596), and VT support from RF grant 14.Z50.31.0004.

#260393 Received 2 Mar 2016; revised 16 Apr 2016; accepted 28 Apr 2016; published 4 May 2016